Scatter Correction for Static CT

Andreas Heinkele[1,2,3], Julien Erath[2], Lukas Hennemann[1,2,3], Joscha Maier[1], Eric Fournié[2], Johan Sunnegaardh[2], Christian Hofmann[2], Martin Petersilka[2], Karl Stierstorfer[2], and Marc Kachelrieß[1,3]

[1]German Cancer Research Center (DKFZ) Heidelberg, Division of X-Ray Imaging and CT, Germany
[2]Siemens Healthineers AG, Computed Tomography Division, Germany
[3]Heidelberg University, Medical Faculty, Germany

GERMAN CANCER RESEARCH CENTER IN THE HELMHOLTZ ASSOCIATION

Research for a Life without Cancer

Introduction

Static CT (see Figure 1) is composed of a stationary detector ring as well as a stationary source ring array. It can be attributed to the family of 4th generation scanners, which were originally rotate-stationary systems with a source moving around the patient.

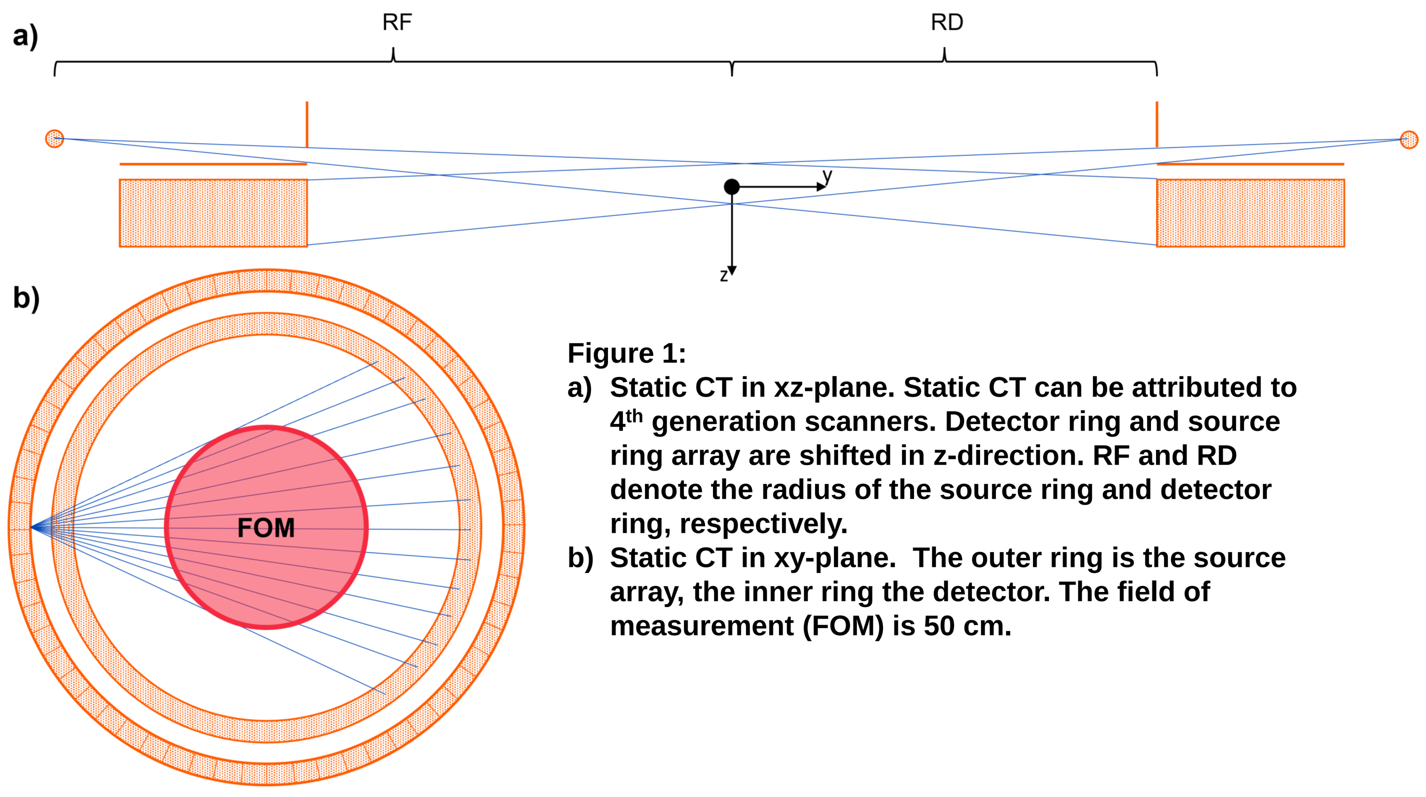

Figure 1:
a) Static CT in xz-plane. Static CT can be attributed to 4th generation scanners. Detector ring and source ring array are shifted in z-direction. RF and RD denote the radius of the source ring and detector ring, respectively.
b) Static CT in xy-plane. The outer ring is the source array, the inner ring the detector. The field of measurement (FOM) is 50 cm.

The design of static CT yields some advantages. For example, by having a stationary detector ring, ring artifacts, which 3rd generation scanners are prone to, can be avoided. Moreover, the absence of rotating components leads to a mechanical simplification and a more compact design. Furthermore, the acquisition time is not limited by the rotation speed of the gantry, but rather by the source power and maximum electronic switching speed between sources. However, the static CT design comes with new challenges. One of the main issues is scattered radiation since the geometry disallows the use of anti-scatter grids (ASGs). This leads to increased noise and artifacts in the image.

Methods

Data generation (see Figure 2)

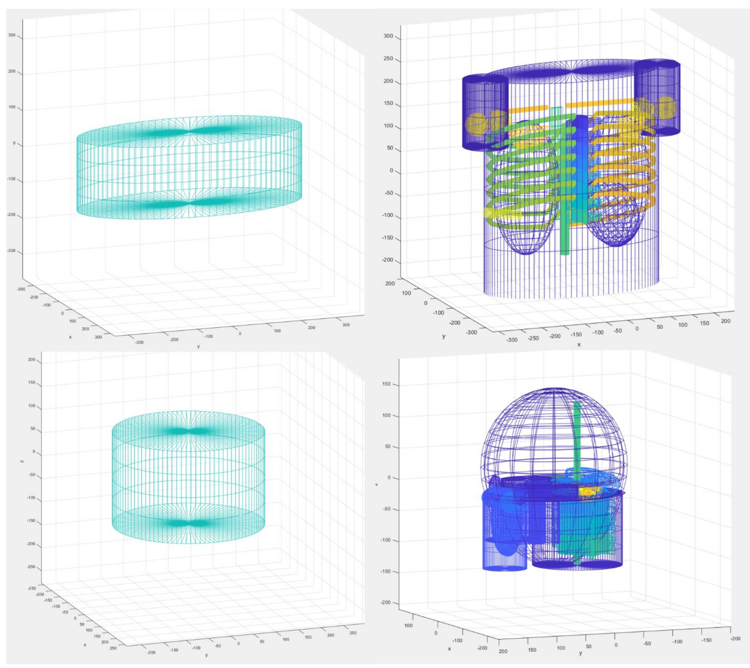

- **Monte-Carlo simulations serve as ground truth (GT)**
- **Network and parameters of a kernel-based comparison method[1] are optimized on our simulated dataset**
- **Training dataset consists of:**
  - **Water phantom ×50**
  - **Ellipse phantom ×50**
  - **Thorax phantom ×100**

  Phantoms differ from each other by simulating with:
  - **Random size**
  - **Random lateral shift up to 8 cm in x and y direction**
  - **Random longitudinal shift (thorax)**
- **Angular steps of 5° simulated**
  - **72 projections per phantom**
- **Train validation split 90:10**

→ A total of 200 phantoms simulated
→ 14400 projections
→ For testing, additional phantoms were simulated (thorax and head)

Figure 2: data generation

Deep Scatter Estimation (DSE)

While kernel-based models underlie physical models with simplified assumptions, DSE[2,3] (see Figure 3) has the advantage that it can learn suitable models without defining them explicitly. DSE is based on a U-net architecture and its weights and biases were determined by minimizing the scatter-to-primary mean absolute percentage error (SPMAPE), since the scatter-to-primary ratio correlates with the scatter artifacts in the resulting image. Two versions of DSE were implemented. A 1-view DSE with 1 projection as input and a 3-view DSE which uses 3 projections as input. DSE can leverage the additional projections to obtain additional 3D information about the object which helps the scatter prediction.

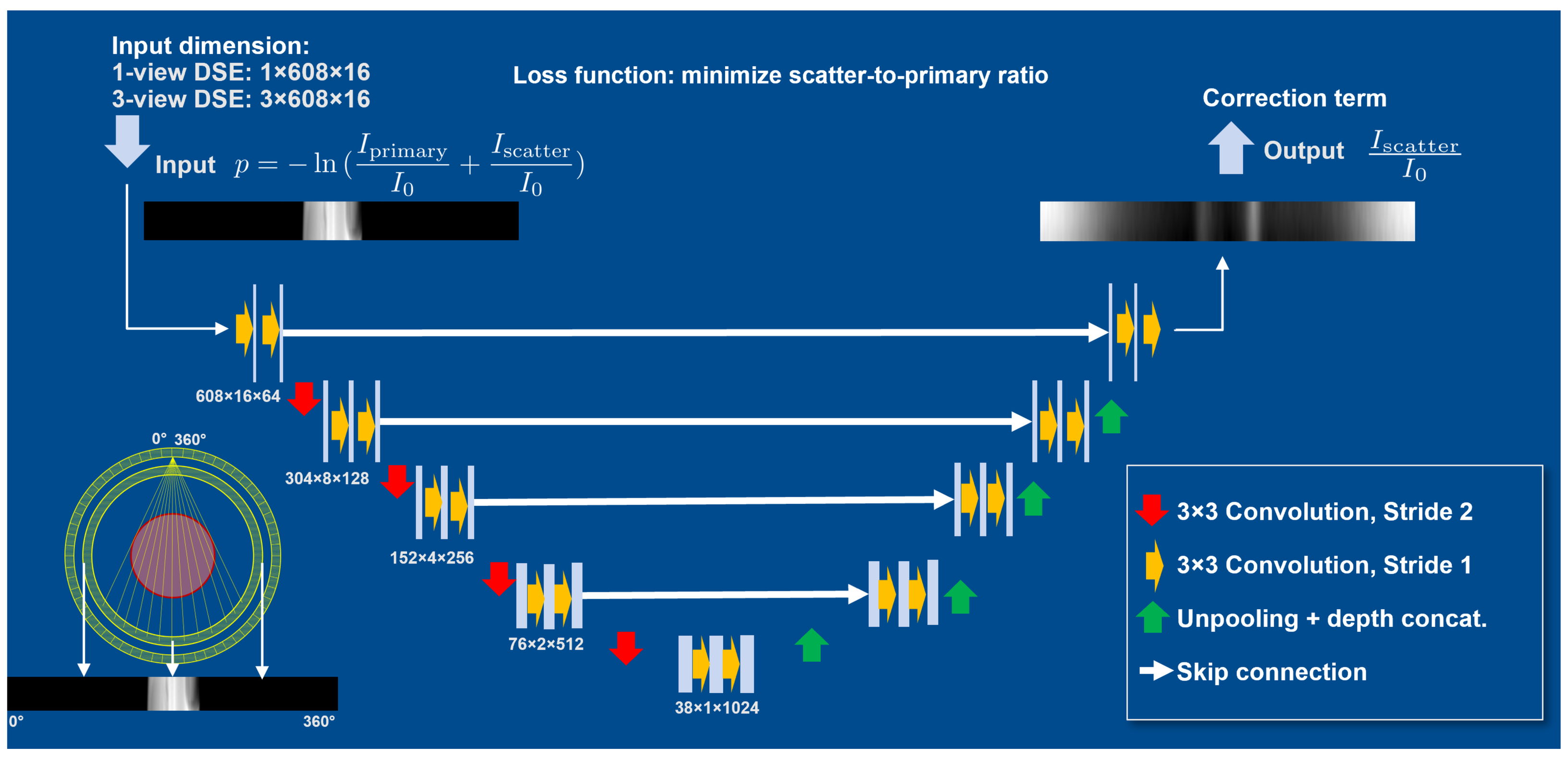

Figure 3: DSE is based on a U-net architecture. The scatter-to-primary mean absolute percentage error (SPMAPE) serves as loss function.

Results

Uncorrected reconstruction of a test thorax phantom (see Figure 4) results in strong scatter artifacts that show up as streaks between regions with high attenuation with a mean absolute error (MAE) of 23.4 HU. Employing 3-DSE, the MAE can be reduced to 0.5 HU. No artifacts remain visible in the reconstruction. On the other hand, the kernel-based method leads to under- or overestimation depending on the region.

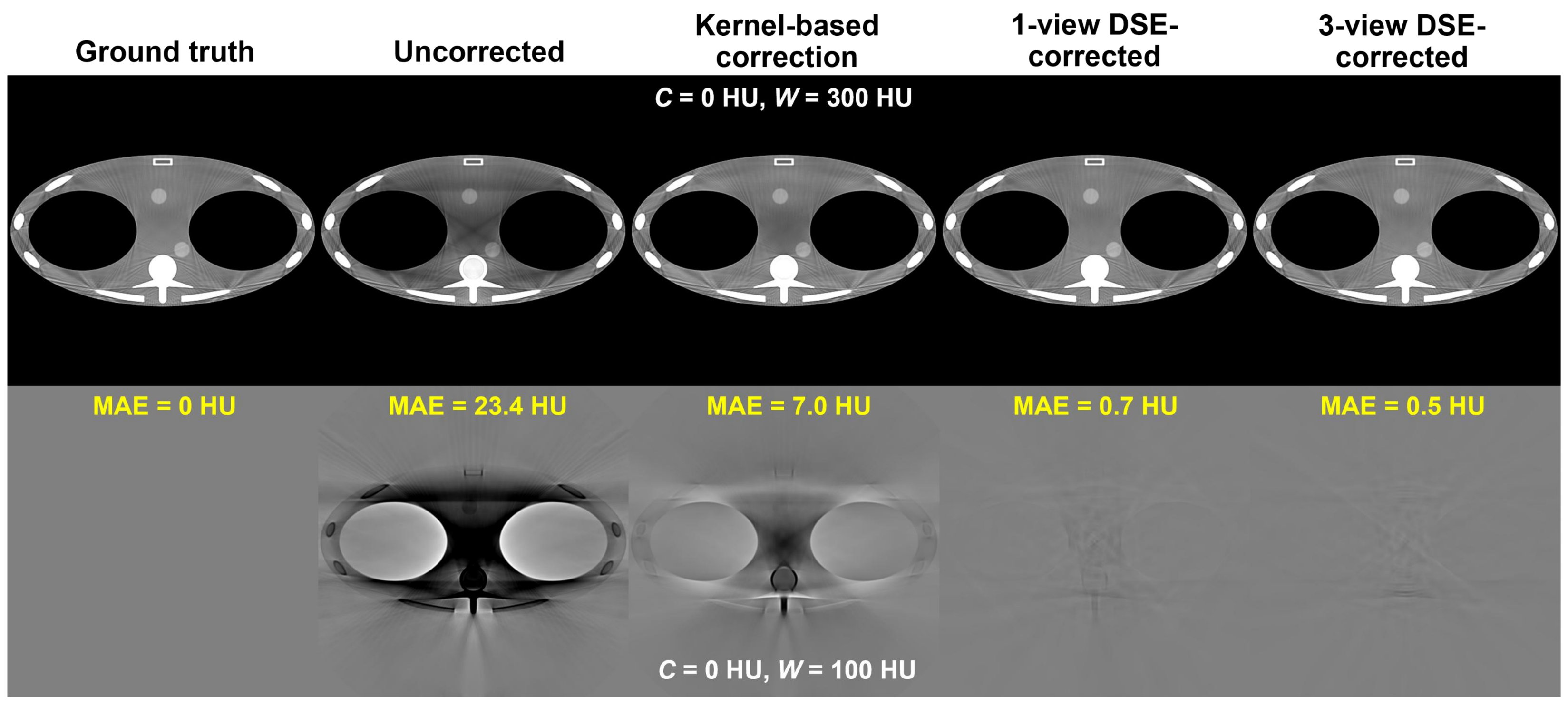

Figure 4: Testing of scatter estimation methods with a simulated thorax phantom. The lowest MAE is achieved by 3-view DSE. Both, 1-view DSE and 3-view DSE outperform the reference method.

Additionally, testing was done on a head phantom (see Figure 5). Although DSE was not trained on any head phantoms, it is able to reduce the MAE from 22 HU to 1.5 HU and outperforms the kernel-based comparison method.

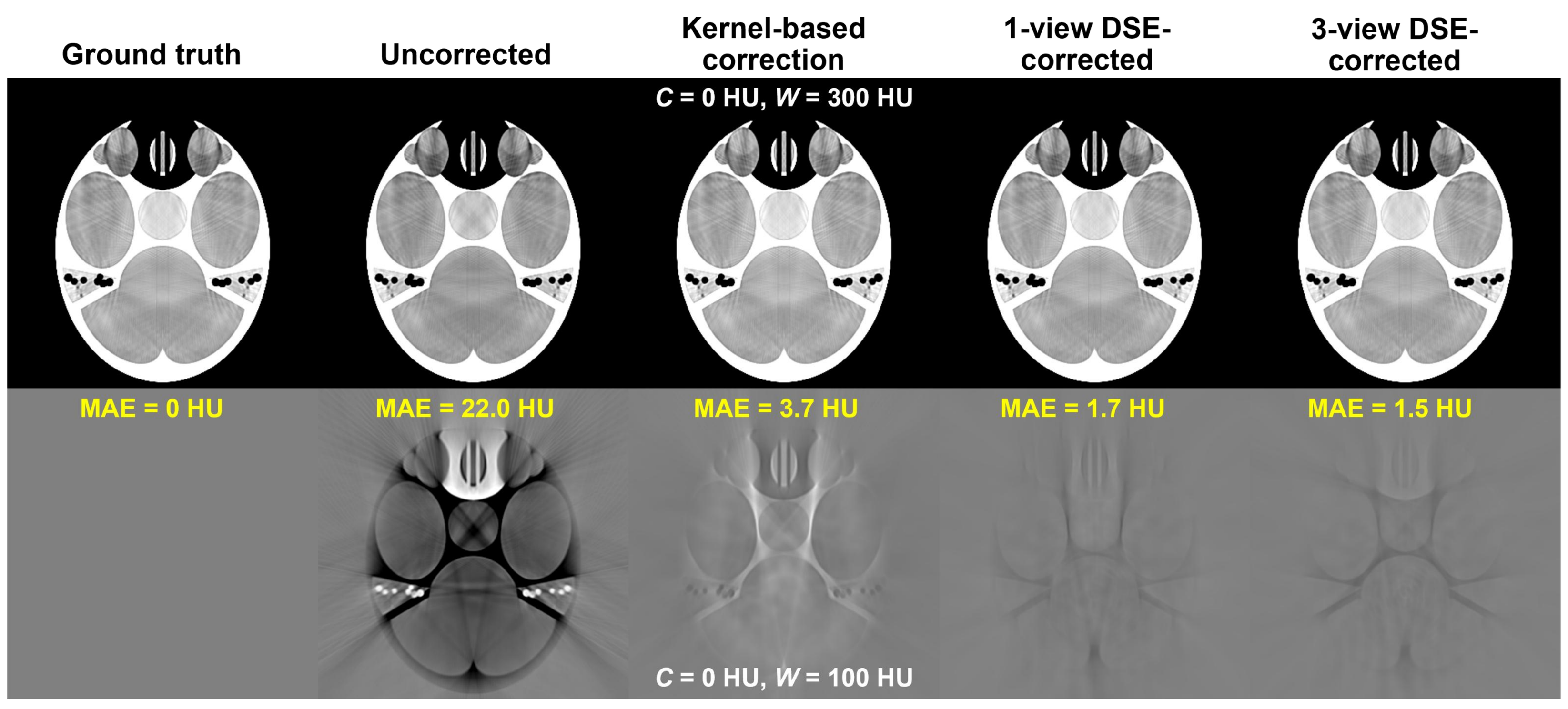

Figure 5: Testing of scatter estimation methods with a simulated head phantom. The lowest MAE is achieved by 3-view DSE. Both, 1-view DSE and 3-view DSE outperform the reference method. The estimation methods were not trained on any head phantoms.

Conclusion

In our simulation study, DSE allows for accurate scatter correction in static CT. This indicates that previous challenges regarding scatter artifacts in 4th generation CT may be overcome using deep learning-based approaches.

[1]Ohnesorge, B., Flohr, T., and Klingenbeck-Regn, K., "Efficient object scatter correction algorithm for third and fourth generation CT scanners," European Radiology 9, 563–569 (Mar. 1999)
[2]Maier, J., Eulig, E., Vöth, T., Knaup, M., Kuntz, J., Sawall, S., and Kachelrieß, M., "Real-time scatter estimation for medical CT using the deep scatter estimation: Method and robustness analysis with respect to different anatomies, dose levels, tube voltages, and data truncation," Medical Physics 46, 238–249 (Nov. 2018)
[3]Erath, J., Vöth, T., Maier, J., Fournié, E., Petersilka, M., Stierstorfer, K., and Kachelrieß, M., "Deep learning-based forward and cross-scatter correction in dual-source CT," Medical Physics 48, 4824–4842 (Aug.2021)